

1 **Topographic control of snowpack**
2 **distribution in a small catchment in the**
3 **central Spanish Pyrenees: intra- and inter-**
4 **annual persistence**

5
6 **J.Revuelto¹, J.I. López-Moreno¹, C. Azorin-Molina¹, S.M. Vicente-Serrano¹**

7
8 ¹ *Instituto Pirenaico de Ecología, Consejo Superior de Investigaciones Científicas (IPE-*
9 *CSIC) Departamento de Procesos Geoambientales y Cambio Global, Campus de Aula Dei,*
10 *P.O. Box 13034, 50059, Zaragoza, Spain*

11
12
13 *Email addresses: jrevuelto@ipe.csic.es, nlopez@ipe.csic.es, cazorin@ipe.csic.es,*
14 *svicen@ipe.csic.es*

15
16
17 * Corresponding author: jrevuelto@ipe.csic.es

22 **Abstract:**

23 In this study we analyzed the relations between terrain characteristics and snow depth
24 distribution in a small alpine catchment located in the central Spanish Pyrenees. Twelve field
25 campaigns were conducted during 2012 and 2013, which were years characterized by very
26 different climatic conditions. Snow depth was measured using a long range terrestrial laser
27 scanner and analyses were performed at a spatial resolution of 5 m. Pearson's r correlation,
28 multiple linear regressions (MLRs) and binary regression trees (BRTs) were used to analyze
29 the influence of topography on the snow depth distribution. The analyses were used to
30 identify the topographic variables that best explain the snow distribution in this catchment,
31 and to assess whether their contributions were variable over intra- and inter-annual time
32 scales. The topographic position index (index that compares the relative elevation of each cell
33 in a digital elevation model to the mean elevation of a specified neighborhood around that cell
34 with a specific shape and searching distance), which has rarely been used in these types of
35 studies, most accurately explained the distribution of snow. The good capability of TPI to
36 predict snow distribution has been observed in both, MLRs and BRTs, for all analyzed days.
37 Other variables affecting the snow depth distribution included the maximum upwind slope,
38 elevation, and northing. The models developed to predict snow distribution in the basin for
39 each of the 12 survey days were similar in terms of the explanatory variables. However, the
40 variance explained by the overall model and by each topographic variable, especially those
41 making a lesser contribution, differed markedly between a year in which snow was abundant
42 (2013) and a year when snow was scarce (2012), and also differed between surveys in which
43 snow accumulation or melting conditions dominated in the preceding days. The total variance
44 explained by the models clearly decreased for those days on which the snowpack was thinner
45 and more patchily. Despite the differences in climatic conditions in the 2012 and 2013 snow
46 seasons, similarities in snow distributions patterns were observed which are directly related
47 with terrain topographic characteristics.

48 **Keywords:** snow depth distribution, snowpack evolution, topography, mountains, cold region

49 **1. Introduction**

50 Assessing the snow distribution in mountain areas is important because of the number of
51 processes in which snow plays a major role, including erosion rates (Pomeroy and Gray,
52 1995), plant survival (Keller et al., 2000; Wipf et al., 2009), soil temperature and moisture
53 (Groffman et al., 2001), and the hydrological response of mountain rivers (Bales and
54 Harrington, 1995; Barnett et al., 2005; Liston, 1999; Pomeroy et al., 2004). As mountain areas
55 are highly sensitivity to global change (Beniston, 2003), snow accumulation and melting
56 processes are likely to be subject to marked changes in coming decades, affecting all
57 processes influenced by the presence of snow (Caballero et al., 2007; López-Moreno et al.,
58 2011, 2012b; Steger et al., 2012). For these reasons, much effort has been devoted to
59 understanding the main factors that control the spatial and temporal dynamics of snow (Egli et
60 al., 2012; López-Moreno et al., 2010; Mott et al., 2010; Schirmer et al., 2011).

61 One of the main difficulties in snow studies is obtaining reliable information of the variables
62 that describe snow distribution, including snow depth (SD), snow water equivalent (SWE)
63 and snow covered area (SCA). Manual measurements have traditionally been used to provide
64 information on the distribution of snowpack, with different sampling strategies having been
65 applied at various spatial scales (Jost et al., 2007; López-Moreno et al., 2012a; Watson et al.,
66 2006). However, manual sampling is not feasible for large areas because of the time involved,
67 especially when SWE measurements are also acquired. In the last decade the use of airborne
68 laser scanners (ALS) (Deems et al., 2006) and terrestrial laser scanners (TLS) (Prokop, 2008),
69 both of which are based on LiDAR (light detection and ranging) technology, have provided
70 for major advances in obtaining data on the SD distribution at unprecedented spatial
71 resolutions. These developments have enabled studies of several factors that in the past have
72 been only marginally considered, including scaling issues (Fassnacht and Deems, 2006; Mott
73 et al., 2011; Schirmer and Lehning, 2011; Trujillo et al., 2007), the detailed dynamics of snow

74 accumulation and ablation (Grünewald et al., 2010; Schirmer et al., 2011; Scipión et al.,
75 2013), and snow transport processes (Mott et al., 2010). In addition, the high density
76 measurements provided by LiDAR technologies are a valuable resource for detailed
77 investigation of the linkage between snow distribution and topography. In the past, this
78 linkage has mostly been studied using manual measurements, and hence with generally
79 limited spatial and temporal resolution (López-Moreno et al., 2010).

80 Previous studies have highlighted the marked control of topography on snow distribution in
81 mountain areas (Anderton et al., 2004; Erickson et al., 2005; Lehning et al., 2011; Mott et al.,
82 2013), and the importance of vegetation and wind exposure (Erxleben et al., 2002; Trujillo et
83 al., 2007). The most commonly used approach has been to develop digital elevation models
84 (DEM) that describe the spatial distribution of elevation, from which other terrain variables
85 are derived such as slope, terrain aspect, curvature, wind exposure or sheltering, and potential
86 solar radiation. This enables to analyze the linear or non-linear relation of these variables to
87 punctual SD or SWE values to be established (Grünewald et al., 2010; Schirmer et al., 2011).

88 Various statistical methods have been applied for this purpose, including linear regression
89 models (Fassnacht et al., 2003; Hosang and Dettwiler, 1991), generalized additive models
90 (GAM) (López-Moreno and Nogués-Bravo, 2005), and binary regression trees (BRT)
91 (Breiman, 1984) which have been widely applied in a diversity of regions (Elder et al., 1991;
92 Erxleben et al., 2002; McCreight et al., 2012).

93 The extent to which topographic variables explain snow distribution can change during the
94 snow season; the variability of terrain characteristics can drive processes related to the spatial
95 variability of snow accumulation (snow blowing, terrain curvature) (Lehning et al., 2008), or
96 affect the energetic exchange between terrain and the snowpack (temperature, incoming solar
97 radiation), so the importance of topographic variables is modified during the season (Molotch
98 et al., 2005). In addition, during a snow season the terrain changes markedly (is smoothed) by
99 snow accumulation (Schirmer et al., 2011). However, few studies have systematically

100 analyzed the intra- and inter-annual persistence of the relation between snow distribution and
101 topography. Recent studies have assessed whether the influence of topography is constant
102 among different years; e.g. the similarities observed at the end of the accumulation season
103 (Schirmer and Lehning, 2011; Schirmer et al., 2011), or the consistent fractal dimensions in
104 two analyzed years (Deems et al., 2008); in both cases there was a relation with the dominant
105 wind direction, which highlights the predictive ability of topographic variables.

106 The main focus of this study was to assess the influence of topography on the spatial
107 distribution of snowpack and its evolution over time. The high temporal and spatial density of
108 the data set collected during the study enabled analysis of the main topographic factors
109 controlling snow distribution, and assessment of whether topographic control of the snowpack
110 varied during the snow season and between years having very contrasting climatic conditions.
111 For this purpose, we conducted 12 surveys over 2012 (6) and 2013 (6) in a small mountain
112 catchment representing a typical subalpine environment in the central Spanish Pyrenees, and
113 obtained high resolution SD measurements using LIDAR technology using a TLS.

114 **2. Study area and snow and climatic conditions**

115 The Izas experimental catchment (42°44'N, 0°25'W) is located in the central Spanish
116 Pyrenees (Fig. 1). The catchment is on the southern side of the Pyrenees, close to the main
117 divide (Spain–France border), in the headwaters of the Gallego River valley, and ranges in
118 elevation from 2000 to 2300 m above sea level. The catchment is predominantly east-facing,
119 with some areas facing north or south, and has a mean slope of 16°. There are no trees in the
120 study area, and the basin is mostly covered by subalpine grasslands dominated by *Festuca*
121 *eskia* and *Nardus stricta*, with rocky outcrops in the steeper areas. Flat, concave and convex
122 areas occur in the basin.

123 The climatic conditions are influenced by the proximity of the Atlantic Ocean, with the
124 winters being humid compared with zones of the Pyrenees more influenced by Mediterranean

125 conditions. The mean annual precipitation is 2000 mm, of which snow accounts for
126 approximately 50% (Anderton et al., 2004). The mean annual air temperature is 3 °C, and the
127 mean daily temperature is < 0 °C for an average of 130 days each year (del Barrio et al.,
128 1997). Snow covers a high percentage of the catchment from November to the end of May.
129 The two years analyzed in the study represent climatic extremes during recent decades.
130 Severe drought occurred during 2012, leading to snow accumulation well below the long-term
131 average. The thickness of the snowpack, measured at the automatic weather station (AWS,
132 Fig. 1), during winter in this year was less than the 25th percentile of the available historical
133 data series of this AWS (1996–2011) (Fig. 2). Only at the end of spring did late snowfall
134 events increase the amount of snow, but this rapidly melted. The opposite occurred in 2013, a
135 year in which the deepest snowpack and the longest snow season of recent decades were
136 recorded. Winter and spring in 2013 were extremely humid, with temperatures mostly
137 between the 25th and 75th percentiles of the AWS historical series. SD accumulation was
138 very high between February and June (exceeding the 75th percentile). In some areas of the
139 basin snow lasted until late July, which is one month longer than in most of the preceding
140 years for which records are available. Regarding net solar radiation data (short wave), no
141 measurements were available before December 2011, However the annual evolution has been
142 tracked on Figure 2 (bottom) showing a clear increase of incoming solar radiation while snow
143 season advance, with high variability due to meteorological factors.

144 **3. Data and methods**

145 **3.1. Snow depth measurements**

146 During the study period high resolution SD maps (Fig. 3) were generated using a long range
147 TLS (Riegl LPM-321), which enables safe acquisition of SD information with short
148 acquisition times from remote areas, compared with measurements obtained manually. This
149 technique has been extensively tested (Prokop et al., 2008; Revuelto et al., 2014; Schaffhauser

150 et al., 2008), and systematically applied to the study of snow distribution in mountain terrain
151 (Egli et al., 2012; Grünewald et al., 2010; Mott et al., 2013; Schirmer et al., 2011). In a
152 previous study the mean absolute error in the most distant areas of the catchment was less
153 than 10 cm (Revuelto et al., 2014), which is consistent with errors reported in previous studies
154 (Grünewald et al., 2010; Prokop, 2008; Prokop et al., 2008; Schaffauser et al., 2008).

155 TLS provides high resolution three dimensional information on the terrain. Nevertheless,
156 error sources need to be considered because they can have large effects on the measurements.
157 To reduce the influences of TLS instability (originated by small displacements of the tripod
158 because TLS vibrations while it is operating), which leads to misalignment with reference
159 points; and atmospheric change, a well-defined protocol must be applied. The protocol
160 applied in this study for generating high resolution SD maps with a 1 m cell size was
161 described by Revuelto et al., (2014). This protocol is based on the following main points: data
162 collection; which includes experimental setup design and information acquisition by the
163 scanning procedure; and data processing, when data is filtered, quality checked and the SD
164 maps generated. Mainly, the methodology was based on differences between DEMs obtained
165 with snow coverage in the study area and a DEM taken at 18 July 2012, when the catchment
166 had no snow cover. Twelve SD maps at a spatial resolution of 5 m were generated for the
167 2012 and 2013 snow seasons (Fig. 3). In each year three surveys were undertaken from
168 February to April (2012: 22 February, 2 April, 17 April; 2013: 17 February, 3 April, 25
169 April), and three were undertaken from May to June when dominated intense melting
170 conditions (2012: 2, 14 and 24 May; 2013: 6, 12 and 20 June). The average SD and SCA, and
171 the maximum SD are shown in Table 1. It shows that much lower SD and SCA were observed
172 in 2012 compared to 2013.

173 **3.2. Digital elevation model and topographic variables**

174 From the two scan stations located in the study area (Fig. 1), 86% of the total area of the
175 catchment was surveyed using the TLS. DEMs of 1 m grid size were initially obtained from

176 point clouds of varying density in different areas, but always with a minimum of 1 point/m²
177 (Revuelto et al., 2014). Some of the predictor variables cannot be calculated where data gaps
178 occur in the DEM (e.g. the topographic position index), and others require a DEM with a
179 greater surface than the area scanned during the study (e.g. to calculate the potential solar
180 radiation, including the shadow effect from surrounding topography, or to calculate the
181 maximum upwind slope parameter, it is included topographic information for distances up to
182 1200 m from the exterior limit of the DEM obtained with the TLS). Thus, a DEM having a 5
183 m grid-size, available from the Geographical National Institute of Spain (Instituto Geográfico
184 Nacional, www.ign.es), was combined with the snow-free DEM obtained using the TLS
185 resampled from 1 m to 5 m resolution (the empty raster of the Geographical National Institute
186 was used for the resampling, averaging all values within each cell). The 1 m grid-size SD
187 maps were also resampled to 5 m to enable matching of the two different data sources.

188 To characterize the terrain characteristics, eight variables were derived from the final DEM,
189 including: (i) elevation (*Elevation* or *Elev.*), (ii) slope (*Slope*), (iii) curvature (*Curvature* or
190 *Curv.*), (iv) potential incoming solar radiation under clear sky conditions (*Radiation* or *Rad.*),
191 (v) easting exposure (*Easting* or *East.*), (vi) northing exposure (*Northing* or *North.*), (vii) the
192 topographic position index (*TPI*) and (viii) maximum upwind slope (*Sx*).

193 *Elevation* was obtained directly from the DEM, while the other variables were calculated
194 using ArcGIS10.1 software. This software calculates *Slope* as the maximum rate of change in
195 value from a specific cell to that of its neighbors (15 x 15 m window size), and *Curvature* is
196 determined from the second derivative of the fitted surface to the DEM in the direction of
197 maximum slope of the terrain for the neighbors cells (15 x 15 m window size too). *Radiation*
198 was obtained using the algorithm of Fu and Rich (2002) and reported in Wh/m² meter based
199 on the average conditions for the 15-day period prior to each snow survey. This algorithm
200 calculates the potential incoming solar radiation (short wave) under clear sky conditions,
201 which may strongly differ from the real radiation as a consequence of cloud cover. This

202 measure provided the relative difference in the extraterrestrial incoming shortwave solar
 203 radiation among areas of the catchment for a given period under given topographical
 204 conditions (Fassnacht et al., 2013). In this way, *Radiation* can be considered as a good proxy
 205 of the spatial distribution of incoming solar energy within the study area. *Easting* and
 206 *Northing* exposure were calculated directly as the sine and cosine, respectively, of the angle
 207 between direction north and terrain orientation or aspect. It provided information on the east
 208 (positive)/west (negative) exposure and the north (positive)/south (negative) exposure.

209 The *TPI* provides information on the relative position of a cell in relation to the surrounding
 210 terrain at a specific spatial scale. Thus, this index compares the elevation of each cell with the
 211 average cell elevation at specific radial distances as follows (De Reu et al., 2013; Weiss,
 212 2001):

$$213 \quad TPI = z_o - \bar{z} \quad (1)$$

$$214 \quad \bar{z} = \frac{1}{n_R} \sum_{i \in R} z_i \quad (2)$$

215 Where z_o is the elevation of the cell in which *TPI* is calculated and \bar{z} is the average elevation
 216 of surrounding cells obtained from (2) for a radial distance R . For each pixel the *TPI* was
 217 calculated for 5, 10, 15, 25, 50, 75, 100, 125, 150 and 200 m radial distances (scale factors).

218 For specific wind directions, the maximum upwind slope parameter, averaged for 45 ° upwind
 219 windows (\overline{Sx} ; Winstral et al., 2002) provided information on the exposure or sheltering of
 220 individual cells at various distances, resulting from the topography. Rather than considering
 221 the contribution for the dominant wind directions (Molotch et al., 2005), \overline{Sx} (Sx further on)
 222 values for eight directions were selected and directly related to the SD. The directions were:
 223 0° for north (N), 45° for northeast (NE), 90° for east (E), 135° for southeast (SE), 180° for
 224 south (S), 225° for southwest (SW), 270° for west (W), and 315° for northwest (NW). For Sx ,
 225 the searching distances (Winstral et al., 2002) considered were 100, 200, 300 and 500 m.
 226 These distances were selected to enable assessment of the range at which Sx exhibited greatest

227 control on SD dynamics, as has occurred in previous studies (Schirmer et al., 2011; Winstral
228 et al., 2002).

229 **3.3. Statistical analysis**

230 The 12 SD maps at 5 m spatial resolution were related to each of the topographic variables
231 considered (including the 40 *Sx* combinations, and the 9 distances for *TPI*). The large number
232 of cells for which SD data were available enabled robust correlations between topography and
233 snow distribution to be obtained, and provided a very large data set for training and validating
234 the SD distribution models.

235 Pearson's *r* coefficients were obtained between SD and each topographic variable. Using the
236 whole data set, each variable was correlated, for all available points, with the SD value for the
237 specific survey day. Given the large amount of data for surveys, the degrees of freedom for
238 correlation analyses were very high and hence they can account for statistically significant
239 correlations even with very low correlation coefficients. Moreover, the use of a very dense
240 data set of observations may have associated problems derived from spatial autocorrelation
241 (Koenig, 1999). For reducing effects derived from spatial autocorrelation we followed a
242 Monte Carlo procedure, in which 1000 random samples of 100 SD cases were extracted from
243 the entire data set (an average of 20,000 SD measurements for each day) and correlated with
244 topographic variables for assessing significance. A threshold 95% confidence interval ($\alpha <$
245 0.05) was used to assess the significance of correlations ($r = \pm 0.197$, based on 100 cases).
246 The spatial scales of *Sx* and *TPI* for which SD showed a higher correlation; 200 m and 25 m
247 respectively, were selected for further analysis (not presented in the manuscript).

248 To assess the explanatory capacity when all topographic variables were considered
249 simultaneously, two statistical models were used: (1) multiple linear regressions (MLRs) and
250 (2) binary regression trees (BRTs). A wide variety of regression analyses for interpretation of
251 much more complex spatial data are available with greater capacity than MLRs and BRTs to
252 deal with spatial autocorrelation issues and the non-linear nature of the relationship between

253 predictors and the response variable (Beale et al., 2010). However, in this study we used
254 MLRs and BRTs because these methods have been and are still widely used in snow studies,
255 and because both enable to isolate accurately the weight of each independent variable within
256 the model, which was the main objective of this research, rather than deriving models with
257 maximum predictive capacity. Prior to run the models a principal component analysis (PCA)
258 was applied to the entire data set for detecting correlations between independent variables that
259 could originate multicollinearity in MLR and BRT. This analysis (not shown) grouped the
260 topographic variables in three components, showing that *TPI* and *Curvature* are highly
261 correlated with PCA component one, and also *Northing* and *Radiation* (but in this case with
262 opposite signs) presented high correlation with component two of the PCA. *TPI* and *Northing*
263 showed both higher correlations with their respective components and in general higher
264 Pearson's r coefficients with SD than *Curvature* and *Radiation* (see result section). Therefore
265 *Curvature* and *Radiation* were discarded as predictors in MLR and BRT analyses.

266 (1) *Multiple linear regression* estimates the linear influence of topographic variables on SD.

267 Despite its simplicity and the rather limited capability under nonlinear conditions (López-
268 Moreno et al., 2010), MLR was used to quantify the relative contribution of each variable
269 to the entire SD distribution model. SD was calculated from the topographic variables at
270 a specific location and day. The threshold for a variable to enter in the model was set at α
271 < 0.05 . Beta coefficients (obtained dividing the standardized units of the coefficients by
272 the mean value of each variable) were used to compare the weight of each variable within
273 the regression models. As a first step, a reduced data set (1,000 cases) was randomly
274 extracted to avoid an excessive number of observations that may lead to spurious
275 identification of statistically significant predictor variables. A stepwise procedure was
276 used to obtain these variables from the random extraction. The variables determined for
277 each survey were used to obtain the final model, but using the entire data set (except
278 5,000 cases for model validation), forcing variables entrance in models.

279 (2) *Binary regression trees* have been widely used to model snowpack distribution from
280 topographic data (Erxleben et al., 2002; Molotch et al., 2005). These are nonparametric
281 models that recursively split the data sample, based on the predictor variable that
282 minimizes the square of the residuals obtained (Breiman, 1984). One BRT was created
283 for each sampling date. The BRTs were run until a new split was not able to account for
284 1% of the explained variance, or when a node had less than 500 cases; a maximum of 15
285 terminal nodes was set, to reduce tree complexity. As there were no over-fitting problems
286 associated with sample size, 15,000 cases were used to grow the trees and 5,000 cases
287 were used for validation. By scaling the explained variance of each variable introduced
288 into each BRT (based on the % of the total explained variance by the BRT), we were able
289 to compare the relative importance of each topographic variable between the different
290 models.

291 Coefficients of determination (r^2) and Willmott's D statistic were used to assess the ability of
292 each model to predict SD over an independent random sample of 5,000 cases. Willmott's D
293 was determined using equation (3) (Willmott, 1981):

$$294 \quad D = 1 - \frac{\sum_{i=1}^N (P_i - O_i)}{\sum_{i=1}^N (|P_i - \bar{O}| + |O_i - \bar{O}|)^2} \quad (3)$$

295 where N is the number of observations, O_i is the observed value, P_i is the predicted value, and
296 \bar{O} is the mean of the observed values. The index ranges from 0 (minimum) to 1 (maximum
297 predictive ability).

298 **4. Results**

299 **4.1. Single correlations**

300 Table 2 shows the correlation between SD and S_x for the eight wind directions at a distance of
301 200 m (identified as the best correlated searching distance in previous analysis). Despite
302 differences in magnitude, the correlations for surveys carried out at the beginning of the
303 season (22 February 2012 and 17 February 2013) in each year showed that SD was clearly

304 affected by N and NW wind directions. The contribution of N and NW wind directions is
305 clearly evident for the surveys on 17 February 2013 (Figure 4, where wind roses with average
306 wind speeds and direction, for the 15 day period before each survey are presented), when
307 greater SD was recorded in the leeward slopes from a northerly direction (Fig. 3, northerly
308 areas of the maps). In the two years of the study a correlation with W and SW wind directions
309 was observed to increase progressively during the snow season (Fig. 4 and Table 2
310 correlations). In 2013 this phenomenon was less marked because of the greater SD
311 accumulation at the beginning of the snow season accompanied with NW direction winds,
312 which resulted in only moderate changes in the S_x for the most strongly correlated wind
313 directions. It was also observed that in both study years once the snow had started to melt (the
314 last three surveys in each season) the snow distribution did not change in relation to S_x
315 directions. The best correlated S_x directions for each survey are in good agreement with wind
316 roses main directions (Fig. 4). These directions for survey days are: 315° for 22 Feb. 2012,
317 270° for 02 and 17 April 2012, and 225° for the three surveys in May 2012; in 2013, 315° was
318 the best correlated direction for 17 Feb. and 270° for the other five surveys of the snow
319 season.

320 Correlations between the best correlated S_x direction for each day and SD were compared
321 with correlations between SD and the other topographic variables (Table 3). This showed that
322 S_x had one of the greatest coefficient of correlation with SD (range 0.22–0.56). The
323 correlations were higher during the accumulation periods, especially in the 2013 snow season,
324 with a reduction in correlations values occurring during the melt period at the end of each
325 snow season.

326 The *TPI* at 25 m showed the highest correlation with SD for the 12 sampled days. During
327 2012 the mean correlation values ranged from -0.32 to -0.58 for those surveys during which
328 snow accumulation dominated in the days preceding the surveys. The r values were closer to
329 the significance level for the surveys where the preceding days were dominated by melting

330 conditions (14 and 24 May). In 2013, the *TPI* was more highly correlated with SD than in
331 2012, with Pearson's r coefficients < -0.6 for all survey days. *Curvature* also had a high
332 correlation with SD, and similar to *TPI* with a 25 m searching distance was significantly
333 correlated on all the survey dates, but unlike the *TPI*, the correlation of *Curvature* with SD did
334 not decrease during the snowmelt periods. The significant correlations of *TPI* and *Curvature*
335 with SD highlight the importance of terrain curvature on the SD distribution. The importance
336 of terrain curvature at different scales for SD distribution is clearly evident in Figure 3, which
337 shows that higher SD values were usually found for concave areas, which showed snow
338 presence until the end of each snow season.

339 The correlation between *Elevation* and SD varied among survey days (Table 3). The
340 correlations were usually positive, but only statistically significant (or approaching
341 significance) for days when melting dominated (the last two surveys in 2012 and 2013). *Slope*
342 was relatively weakly correlated with SD during the 2012 snow season. In 2013 the
343 correlation was greater, and was statistically significant for all days. Similarly to *Elevation*,
344 the correlation between *Slope* and SD was variable between the two study years, and showed
345 a similar temporal pattern to *Easting*, probably because of the presence of steeper areas on the
346 east-facing slopes.

347 The correlation between *Northing* and SD was rarely statistically significant, highly variable
348 and contributed to explaining SD in a very different ways in 2012 and 2013. In 2012 no
349 correlation between SD and *Northing* was found during the accumulation period, but during
350 the melting period a slight positive correlation was observed, as snow remained longer on
351 north-facing slopes. The 2013 snow season started with a large precipitation event dominated
352 by strong winds from a northerly direction, leading to high levels of snow accumulation on
353 the south-facing slopes. This explains the strong and statistically significant negative
354 correlation of SD with *Northing* for 17 February 2013. This event influenced the rest of the
355 season (as evident in Table 2 for 2013), but a progressive decrease in its influence was

356 evident for the following survey days. *Radiation* had an almost opposite influence on SD to
357 that observed for *Northing*. During the melting period in each year the Pearson's r correlation
358 between SD and *Radiation* was negative, indicating a thinner snowpack on the most irradiated
359 slopes. This relation was statistically significant at the end of the 2013 snow season.
360 However, during the accumulation period in 2013 statistically significant and positive
361 correlations were observed with *Northing* and *Radiation*, which are connected to the strong
362 snow redistribution by winds from N-NW directions.

363 **4.2. Multiple Linear Regression and Binary Regression Tree models**

364 Figure 5 shows the Willmott's D values and the coefficients of determination (r^2) obtained in
365 the comparison of observed and predicted values using MLRs and BRTs for a data set
366 reserved for validation (5000 cases). The MLRs produced r^2 values ranging from 0.25 to 0.65
367 and Willmott's D values ranging from 0.60 to 0.88, while the BRTs produced r^2 values
368 ranging from 0.39 to 0.58 and Willmott's D values ranging from 0.72 and 0.85. For both
369 methods the relations between the observed and predicted values was stronger for 2013.
370 Accuracy decreased at the end of the snow season, when the snowpack was mostly patchy
371 across the basin; this was particularly the case for the end of the 2012 season. Overall, the
372 performance of the MLRs was more variable than that of the BRTs, which were more
373 constant amongst the various snow surveys. For those days on which the models were most
374 accurate in predicting SD variability, the MLRs showed slightly better scores than the BRTs.
375 However, for days on which the accuracy between predictions and observations was lower,
376 the BRTs provided better estimates than the MLRs. For 2012, slightly better results were
377 obtained using MLRs, while the opposite occurred in 2013. Nevertheless, only large
378 differences in the accuracy of each model were evident by the end of 2012 snow season, in
379 the two last surveys, which were characterized by thin and patchy snowpack.

380 As shown for single correlations, the *TPI* variable explained most of the variance in MLR
381 models developed for all analyzed days (Table 4). The contribution of the other variables

382 varied markedly among surveys, particularly when the two years were compared. In most
383 cases, *Elevation* was the second most important variable explaining the SD distribution in
384 2012, followed by *Sx* and *Slope*. The other variables made a much smaller contribution, or
385 were not included in the models. The contribution of *Elevation* was much less in 2013, and it
386 was not included in three of the six surveys, whereas in 2012 it was included in all surveys.
387 For the entire 2013, *Sx* was the second most important variable, followed by *Easting*, which
388 had an almost negligible influence in 2012. *Northing* was only included in the models for the
389 surveys carried out during periods dominated by snow accumulation, and was not included in
390 the models during the periods dominated by melting.

391 Figure 6 shows two examples of BRTs, obtained for the days 2 May 2012 (upper panel) and 3
392 April 2013 (bottom panel), which accounted for the largest amount of snow accumulation in
393 both years. The variable *TPI* determined the first branching point, and this occurred in the
394 majority of the trees obtained (not shown). After the first branching, other variables were
395 significant in the model, including *Sx* and *TPI* for 2 May 2012, and *Sx* and *Northing* for 3
396 April 2013, demonstrating the importance of these variables in the subsequent branching of
397 the trees.

398 The relative importance (scaled from 0 to 100) of each topographic variable in each BRT is
399 shown in Table 5. This shows that *TPI* was the first most important variable explaining SD
400 for all survey days. For the 2012 snow season, *TPI* explained more than 67% of the total
401 explained variance in all BRTs, and 75% during the accumulation period (the first three
402 surveys). Thus, for most of the survey days the variance explained by the other variables was
403 < 30%. Besides *TPI* was in all cases the first split variable (which accounted from a 23 to a
404 30% of the explained variance), with a critical value that ranged from -0.67 m to -0.43 m and
405 an average value of -0.54 m. The second most important variable explaining the SD
406 distribution in 2012 differed amongst survey days. Thus, *Sx* was the second most influential
407 variable during May (except for 24 May 2012), following the largest snowfall in the season

408 (which occurred the 1 May 2012), and *Elevation* was the most important variable in the other
409 surveys during 2012. *Northing* also had an evident influence during the two first surveys of
410 the year, but subsequently had minimal explanatory capacity, as was the case for all the other
411 variables. In 2013 *TPI* was also the main contributor to the total explained variance,
412 exceeding 50% for almost all survey days, and approaching or > 70% during the snowmelt
413 period. For this year, also *TPI* was the first split variable in nearly all BRT, with critical
414 values ranging from -0.47 m to -0.15 m and an average value of -0.28 m; except for the 13
415 February 2013, in which *Sx* was the first split variable. The influence of *Sx* was more
416 important in 2013 than in the previous year. At the beginning of 2013 the contribution of *Sx* to
417 the total explained variance was almost 46%, and remained > 20% for the rest of the snow
418 season. An exception was the last survey, when melting dominated and its effect declined to
419 12%. When snow was not mobilized for long periods by wind (no changes on the best
420 correlated wind direction of *Sx* are observed), the SD distribution was more dependent on
421 variables related to terrain curvature (*TPI* and *Curvature*). During 2013, *Elevation* contributed
422 approximately 5% to the total explained variance during the entire snow season. *Northing*
423 made a significant contribution to the model (14.7%) only one day (3 April 2013), and a
424 smaller contribution on the following survey day (25 April 2013). When included in the
425 BRTs, the other variables (*Easting*, *Radiation*) made minor, contributions to the total
426 explained variance.

427 Figure 7 shows the mean contribution of each topographic variable versus the coefficient of
428 variation from the twelve surveys for the different statistical approaches considered in this
429 study (Pearson's r coefficients, beta coefficients of the MLRs and the contribution to the
430 explained variance for each BRT). Clearly, *TPI* is the most important variable to explain the
431 snow distribution in the catchment, but it is also the variable that exhibits a lower variability
432 between the different surveys ($CV < 0.2$). Besides it has been introduced as predictor for MLRs
433 and BRTs in all studied days. *Sx* is the next variable in importance to explain snow

434 distribution, being introduced as predictor in the majority of the modelled days (11 and 10 out
435 of 12 days for MLRs and BRTs respectively). It shows a low temporal variability when
436 correlation's coefficients are calculated (CV=0.24), but the variability in its contribution to
437 MLRs and BRTs increases noticeably, with CV values of 0.35 and 0.59 respectively. The rest
438 of the variables show a much lower mean contribution for explaining snow distribution and a
439 high temporal variability in their explanatory role. Lower CV values are observed for MLRs,
440 ranging the majority between 0.3 and 0.4, than for BRTs models, ranging the majority
441 between 0.4 and 0.8.

442 **5. Discussion**

443 The distribution of snow in mountain areas is highly variable in space and time, as shown for
444 Izas experimental catchment during two consecutive years. Many meteorological and
445 topographic parameters affect the snow distribution and its evolution through time with
446 different weights subjected to several factors. In this context, we demonstrated that terrain
447 characteristics significantly affect SD distribution in a subalpine catchment. Also we have
448 showed that its effect evolved during the snow accumulation and melting periods over two
449 years having highly contrasting climatic conditions and snow accumulation amounts

450 Many studies have analyzed the spatial distribution of SD in mountain areas considering both,
451 intra- and inter- annual variability of the topographic control on the snowpack distribution
452 (Anderton et al., 2004; Erickson et al., 2005; López-Moreno et al., 2010; McCreight et al.,
453 2012). Other researches have also focused their attention in long-term inter-annual snow
454 distribution analyses (Jepsen et al., 2012; Sturm and Wagner, 2010; Winstral and Marks,
455 2014). The results of these previous works have highlighted the difficulties in fully explaining
456 the distribution of snow in complex mountainous terrain. In addition, results differ among
457 studies, and suggest that different variables govern the distribution of snowpack among areas
458 as consequence of their different characteristics and geographical settings. These differences
459 include surface extension, the altitudinal gradients, the importance of wind redistribution, the

460 presence or absence of vegetation and the topographic complexity as concluded by
461 Grünewald et al., (2013) in a study where seven study sites across the world were considered.

462 Most of the topographic variables investigated in this study have been included in previous
463 studies, including *Elevation*, *Slope*, *Radiation*, *Curvature* and *Sx*. Other variables, in
464 particular *TPI*, have received little attention in previous research (López-Moreno et al., 2010).
465 We showed that *TPI* at a scale of 25 m had the greatest capacity to explain the SD distribution
466 in the study catchment. *Curvature* (which refers to a smaller spatial scale of terrain curvature
467 when compared with *TPI*) is also highly correlated with the SD distribution, but not as much
468 as *TPI*. This reinforces the importance of considering terrain curvature at various scales for
469 explaining the SD distribution in mountain environments. The correlation between snowpack
470 and the *TPI* decreased during melting periods, whereas the correlation with *Curvature*
471 remained constant. This suggests that snow accumulates more in small, deep concavities, but
472 is shallower at the end of the season in wider concave areas that were identified by the 25 m
473 *TPI* scale. This effect was evident at the end of the snow season, when snow was present only
474 in deep concavities, as shown in Figure 3. To explain the snow distribution, Anderton et al.
475 (2004) compared the relative elevation of a cell with the terrain over a 40 m radius, and
476 observed that this had a major role on SD distribution, what sustain curvature importance at
477 different scales.

478 The maximum upwind slope (*Sx*; Winstral et al., 2002) has also been identified as a key
479 variable explaining snow distribution, improving the results obtained when it is introduced
480 into models. Our results, 200 m searching distance for *Sx*, is comparable with those of other
481 studies that have shown that the optimum searching distance for correlating *Sx* with the SD
482 distribution is 300 m (Schirmer et al., 2011), which is not a large difference for the considered
483 distances in this work reaching 500 m. As it is observed from the reported wind information,
484 Izas experimental catchment has W-NW dominant wind direction what is consistent with the
485 best correlated *Sx* directions. For this reason, the *Sx* preferred direction for each date was

486 selected, and showed that there were intra-annual shifts in the most highly correlated
487 direction. The change in the most important *Sx* direction was similar between the 2012 and
488 2013 snow seasons; it started with a northerly component and evolved to a dominant westerly
489 direction. We also found a decrease in the correlation between *Sx* and the snow distribution at
490 the end of each snow season, when melting conditions dominated. This is consistent with the
491 findings of previous studies (Winstral and Marks, 2002).

492 *Sx* parameter takes into account sheltering effects with topographic origin in relation to wind
493 directions. SD distribution maps show higher SD amounts in leeward slopes, located in E-SE
494 slopes. *TPI* is not able to explain snow drifts, because this index considers the topographic
495 characteristics in all directions. Nevertheless, terrain characteristics at the study site in relation
496 to SD distribution have shown a higher importance of *TPI* when compared to *Sx*. The most
497 plausible explanation accounting for this result is that the basin has a rather reduced size,
498 shows the same general aspect (SE facing) and topography is relatively gentle. Under such
499 conditions, during wind blowing events snow is accumulated in all wide concavities of the
500 basin (represented by *TPI*) independently of its specific location. Nonetheless, wind
501 redistribution will be affected by a combination of local topography and main wind
502 directions; which makes necessary to consider the *Sx* parameter. As it has been observed, this
503 effect lasts in time until the melting season is advanced.

504 Only for two days (22 February 2012 and 2 April 2012) was there no (or a minor)
505 contribution of *Sx* to explain SD distribution, according to BRTs and MLRs. On these days
506 *Northing* was introduced into the models, and was found to explain some of the variance of *Sx*
507 from northerly direction (the best correlated direction for these days (Table 2)).

508 Although *Elevation* has been found to largely explain the snow distribution in areas having
509 marked altitudinal differences (Elder et al., 1998; Erxleben et al., 2002; Molotch and Bales,
510 2005) in our study no strong association was found between SD and *Elevation*, with
511 significant correlations occurring only during the snowmelt period. This is because of the low

512 elevation range of the study area (300 m). During the accumulation period the entire
513 catchment is generally above the freezing height. However, during spring the 0°C isotherm
514 shifts to higher elevations, which may lead to different melting rates within the basin. Despite
515 the relatively weak correlation between *Elevation* and SD, this variable was introduced as a
516 predictor in the MLRs and BRTs for most of the days analyzed. Similarly, López-Moreno et
517 al. (2010) reported that elevation was of increasing importance as the grid size increased.
518 Anderton et al. (2004) also informed about the importance of elevation to explain snowpack
519 distribution in the same study area. The results of the present study suggest the increase in
520 importance of *Elevation* at the end of the snow season, and particularly when it is considered
521 in combination with other topographic variables in MLR and BRT models.

522 *Slope* has a weak explanatory factor for snow distribution, probably because the slope in most
523 of the catchment is not steep enough to trigger gravitational movements including avalanches
524 and slushes during the snowmelt period, which could thin the snowpack on the steepest slopes
525 (Elder et al., 1998). Most likely some of *Slope* explanatory capacity is included on *Radiation*
526 explanatory capacity, because it affects solar light incident angle, besides the steeper areas of
527 the catchment are in south facing zones. Nevertheless quantifying such kind of effects is
528 highly difficult due to the high complexity of SD dynamic in mountain terrain.

529 *Radiation*, *Northing* and *Easting* showed no close correlation with the snowpack distribution;
530 their relationships with SD were variable over time, with statistically significant correlations
531 occurring on some days and only weak correlations on other days. The results suggested that
532 *Radiation* and *Northing* (which showed almost opposite patterns) may be related to SD for
533 two different reasons. During the accumulation period in 2013 heavy snowfalls associated
534 with northerly winds led to the accumulation of deep snow on south-facing (more irradiated)
535 surfaces, whereas during the snowmelt period the greater exposure of the southern slopes to
536 solar energy led to a positive (negative) correlation with *Northing* (*Radiation*). This
537 phenomenon was also observed by López-Moreno et al. (2013), using a physically-based

538 snow energy balance model in the same study area. Moreover, the high and opposite
539 correlation between *Northing* and *Radiation* obtained in PCA results (not shown in the
540 manuscript), was showing a potential problem of multicollinearity. Thus, only *Northing* was
541 considered for MLRs and BRTs (the same occurred with *TPI* and *Curvature*, being only
542 considered in statistical models the *TPI*). Although *Northing* did not show a significant
543 correlation with SD during accumulation periods; when the surveys were closer to the
544 snowmelt period, the negative correlation of this variable with SD was more evident, possibly
545 due to the increase of the difference in the energetic exchange between sun exposed and
546 shaded areas. The importance of *Northing* in MLR models, combined with the contribution of
547 *Easting* during the accumulation period may be related to the high snow redistribution
548 originated by wind directions from N- NW directions. Therefore terrain aspect relation with
549 SD distribution (considered with *Northing* and *Easting*) in winter is tightly related to the
550 accumulation patterns resulting from wind redistribution, whereas in spring they were
551 associated with the unequal distribution of solar radiation, which leads to higher melting rates
552 on the most irradiated slopes, what has shown better explanatory capacity than *Radiation* at
553 Izas Experimental catchment.

554 The MLRs and BRTs provided reasonably high accuracy scores when observed and predicted
555 SD data were compared. The scores were comparable, and in some cases better, to values
556 reported in previous researches using similar methods. As an example, Molotch et al., (2005)
557 reported r^2 values between 0.31 and 0.39 using BRT; and Winstral et al., (2002), who
558 considered different number of terminal nodes of BRT, obtained an optimal tree size of 16
559 nodes data set with an r^2 value close to 0.4. Moreover results presented here were obtained
560 from a separate data set, and data used to create the models were not considered for testing,
561 thanks to the large available data set. One reason for the improvement may be the use of the
562 *TPI* as a SD predictor, as this variable has not been considered in previous studies.
563 Nevertheless, it should be noted that the study sites considered in other studies, could differ in

564 terms on complexity of terrain, and also in SD accumulation amounts. For the 12 survey days
565 the *TPI* had the greatest explanatory capacity in both approaches. However, based on
566 comparison of the different dates and surveys, the other variables made more varying
567 contributions, as a result of the different roles they play during the snow accumulation and
568 melting periods, and the wind conditions during the main snowfall events. The models had
569 less capacity to explain spatial variability of the snowpack when the snow was thinner and
570 patchy. The BRT and MLR approaches were consistent with respect to error estimates. The
571 results obtained using each approach were comparable, so the trends in the variable ranking
572 with both models for each survey day were similar. Only during conditions of snow scarcity
573 did the BRT approach demonstrate better capability to relate SD to topography. This is
574 probably a consequence of the greater capacity of BRTs to take account of the nonlinear
575 response of the snowpack to topography, and the occurrence of sharp thresholds typical of
576 days when the snowpack is patchy (López-Moreno et al., 2010; Molotch et al., 2005).

577 **Despite model results differ between survey days and years, the most important variable, *TPI*,**
578 **is always present in the models and their contribution to the total explained variances show**
579 **very low CV values.** Other variables with an also important role to explain SD distribution
580 (i.e. S_x) are included in most of the models as predictors showing their influence on snowpack
581 distribution, although their contribution to the final models changes noticeably amongst
582 different surveys. Moreover for 2012 and 2013 a consistent inter-annual distribution of the
583 snowpack in the catchment is observed; the areas of maximum SD and the location of snow
584 free zones were consistent between both years of the study, and more importantly there is a
585 strong consistency of the effect of topography on SD. This spatial consistency of snowpack
586 has implications for soil dynamics and plant cycles, because some parts of the basin will tend
587 to remain free of snow cover during longer periods favoring the presence of temporary frozen
588 soils, and reducing the isolation effect of snowpack to the plants (Keller et al., 2000; Pomeroy
589 and Gray, 1995). Besides, it suggests that the information acquired from TLS during several

590 years could be useful to design long-term monitoring strategies of SD in the basin based on
591 few manual measurements in representative points according their terrain characteristics.

592 **6. Conclusions**

593 The *TPI* at a 25 m searching distance was the best topographic variable, and the most
594 persistent in time, for explaining SD distribution in the Izas experimental catchment. This
595 suggests the importance of including this index in future snow studies, and the need to
596 establish the best searching distance for relating this variable to SD distribution at other study
597 sites. The maximum upwind slope (*Sx*) at a searching distance of 200 m was also an important
598 variable explaining the SD distribution, but its influence varied markedly between years and
599 surveys, depending of the specific wind conditions during and after main snowfall events.
600 Nevertheless, *Sx* has shown a similar evolution pattern for the best correlated direction in the
601 two analyzed snow seasons. The influence of the other topographical variables on the spatial
602 distribution of SD was lower, and showed higher intra- and inter-annual variability. The total
603 variance explained by BRTs and MLRs clearly decreased for periods on which the snowpack
604 was thinner and more patchily. The results from BRTs and MLRs models were consistent in
605 terms of variables importance ranking, and the explanatory capacities of the main variables
606 were similar for all surveys. Except *TPI*, that showed very low coefficient of variations for the
607 two approaches, the variability of the contribution of each topographic variable for the
608 different surveys was noticeably lower for MLRs than for BRTs.

609 **7. Acknowledgments**

610 This study was supported by the research project “Hidrología nival en el Pirineo Central
611 Español: Variabilidad espacial, importancia hidrológica y respuesta a la variabilidad y cambio
612 climático (CGL2011-27536/HID, Hidronieve)” CGL2011-27574-CO2-02 and CGL2011-
613 27536, financed by the Spanish Commission of Science and Technology and FEDER; LIFE
614 MEDACC, financed by the LIFE programme of the European Commission; “El glaciar de

615 Monte Perdido: Monitorización y estudio de su dinámica actual y procesos criosféricos
616 asociados como indicadores de procesos de cambio global 844/2013, financed by
617 MAGRAMA National Parks and CTP1/12 “Creación de un modelo de alta resolución
618 espacial para cuantificar la esquiabilidad y la afluencia turística en el Pirineo bajo distintos
619 escenarios de cambio climático”, financed by the Comunidad de Trabajo de los Pirineos. The
620 first author is a recipient under the pre-doctoral FPU grant program 2010 (Spanish Ministry of
621 Education Culture and Sports). The third author was the recipient of the postdoctoral grants
622 JAE-DOC043 (CSIC) and JCI-2011-10263 (Spanish Ministry of Science and Innovation).
623 The authors thank Adam Winstral for the use of his algorithm for calculating maximum
624 upwind slope. The authors wish to acknowledge the editor and the two reviewers for their
625 detailed and helpful comments to the original manuscript.

626 **8. References**

- 627 Anderton, S.P., White, S.M., and Alvera, B.: Evaluation of spatial variability in snow water
628 equivalent for a high mountain catchment. *Hydrol. Process.*, 18, 435–453, 2004.
- 629 Bales, R.C., and Harrington, R.F.: Recent progress in snow hydrology. *Reviews of*
630 *Geophysics Supplement*, 33, 1011–1020, 1995.
- 631 Barnett, T.P., Adam, J.C., and Lettenmaier, D.P.: Potential impacts of a warming climate on
632 water availability in snow-dominated regions. *Nature*, 438, 303–309, 2005.
- 633 Del Barrio, G., Alvera, B., Puigdefabregas, J., and Diez, C.: Response of high mountain
634 landscape to topographic variables: Central pyrenees. *Landscape Ecol.*, 12, 95–115, 1997.
- 635 Beale, C.M., Lennon, J.J., Yearsley, J.M., Brewer, M.J., and Elston, D.A.: Regression
636 analysis of spatial data. *Ecol. Lett.*, 13, 246–264, 2010.
- 637 Beniston, M.: Climatic Change in Mountain Regions: A Review of Possible Impacts. *Climatic*
638 *Change*, 59, 5–31, 2003.
- 639 Breiman, L.: *Classification and regression trees* (Wadsworth International Group). 1984.

640 Caballero, Y., Voirin-Morel, S., Habets, F., Noilhan, J., LeMoigne, P., Lehenaff, A., and
641 Boone, A.: Hydrological sensitivity of the Adour-Garonne river basin to climate change.
642 *Water Resour., Res.* 43, W07448, 2007.

643 De Reu, J., Bourgeois, J., Bats, M., Zwertvaegher, A., Gelorini, V., De Smedt., P.M., Chu,
644 W., Antrop., M., De Maeyer, P., Finke., P., Mairvanne, M.V., Verniers., J. and Crombé., P.:
645 Application of the topographic position index to heterogeneous landscapes. *Geomorphology.*
646 186 , 39-49. 2013.

647 Deems, J.S., Fassnacht, S.R., and Elder, K.J.: Fractal Distribution of Snow Depth from Lidar
648 Data. *J. Hydrometeorol.*, 7, 285–297, 2006

649 Deems, J.S., Fassnacht, S.R., and Elder, K.J.: Interannual Consistency in Fractal Snow Depth
650 Patterns at Two Colorado Mountain Sites. *J. Hydrometeorol.* 9, 977–988, 2008

651 Egli, L., Jonas, T., Grünewald, T., Schirmer, M., and Burlando, P.: Dynamics of snow
652 ablation in a small Alpine catchment observed by repeated terrestrial laser scans. *Hydrol.*
653 *Process.*, 26, 1574–1585. 2012.

654 Elder, K., Dozier, J., and Michaelsen, J.: Snow accumulation and distribution in an Alpine
655 Watershed. *Water Resour. Res.*, 27, 1541–1552. 1991.

656 Elder, K., Rosenthal, W., and Davis, R.E.: Estimating the spatial distribution of snow water
657 equivalence in a montane watershed. *Hydrol. Process.* 12, 1793–1808, 1998.

658 Erickson, T.A., Williams, M.W., and Winstral, A.: Persistence of topographic controls on the
659 spatial distribution of snow in rugged mountain terrain, Colorado, United States. *Water*
660 *Resour. Res.*, 41 (4), 1–17, 2005.

661 Erxleben, J., Elder, K., and Davis, R.: Comparison of spatial interpolation methods for
662 estimating snow distribution in the Colorado Rocky Mountains. *Hydrol. Process.*, 16, 3627–
663 3649, 2002.

664 Fassnacht, S.R., and Deems, J.S.: Measurement sampling and scaling for deep montane snow
665 depth data. *Hydrol. Process.*, 20, 829–838, 2006.

666 Fassnacht, S.R., Dressler, K.A., and Bales, R.C.: Snow water equivalent interpolation for the
667 Colorado River Basin from snow telemetry (SNOTEL) data. *Water Resour. Res.*, 39 (8),
668 SWC31–SWC310, 2003.

669 Fassnacht, S.R., López-Moreno, J.I., Toro, M., and Hultstrand, D.M.: Mapping snow cover
670 and snow depth across the Lake Limnopolar watershed on Byers Peninsula, Livingston Island,
671 Maritime Antarctica. *Antarct. Sci.*, 25, 157–166, 2013.

672 Fu, P., and Rich, P.M.: A geometric solar radiation model with applications in agriculture and
673 forestry. *Computers and Electronics in Agriculture*, 37, 25–35, 2002.

674 Groffman, P.M., Driscoll, C.T., Fahey, T.J., Hardy, J.P., Fitzhugh, R.D., and Tierney, G.L.:
675 Colder soils in a warmer world: A snow manipulation study in a northern hardwood forest
676 ecosystem. *Biogeochemistry*, 56, 135–150, 2001.

677 Grünewald, T., Schirmer, M., Mott, R., and Lehning, M. Spatial and temporal variability of
678 snow depth and ablation rates in a small mountain catchment. *The Cryosphere*, 4, 215–225,
679 2010.

680 Grünewald, T., Stötter, J., Pomeroy, J.W., Dadic, R., Moreno Baños, I., Marturià, J., Spross,
681 M., Hopkinson, C., Burlando, P., and Lehning, M.: Statistical modelling of the snow depth
682 distribution in open alpine terrain. *Hydrol. Earth Syst. Sci.*, 17, 3005–3021. 2013

683 Hosang, J., and Dettwiler, K.: Evaluation of a water equivalent of snow cover map in a small
684 catchment area using a geostatistical approach. *Hydrol. Process.*, 5, 283–290., 1991.

685 Jepsen, S.M., Molotch, N.P., Williams, M.W., Rittger, K.E., and Sickman, J.O.: Interannual
686 variability of snowmelt in the Sierra Nevada and Rocky Mountains, United States: Examples
687 from two alpine watersheds. *Water Resour. Res.* 48, W02529, 2012.

688 Jost, G., Weiler, M., Gluns, D.R., and Alila, Y.: The influence of forest and topography on
689 snow accumulation and melt at the watershed-scale. *Journal of Hydrology*, 347, 101–115,
690 2007.

691 Keller, F., Kienast, F., and Beniston, M.: Evidence of response of vegetation to environmental
692 change on high-elevation sites in the Swiss Alps. *Reg. Environ. Change*, 1, 70–77, 2002.

693 Koenig, W.D.: Spatial autocorrelation of ecological phenomena. *Tends in Ecology &*
694 *Evolution*, 14, 1 22-26, 1999.

695 Lehning, M., Löwe, H., Ryser, M., and Raderschall, N.: Inhomogeneous precipitation
696 distribution and snow transport in steep terrain. *Water Resour. Res.*, 44, W07404, 2008.

697 Lehning, M., Grünewald, T., and Schirmer, M. : Mountain snow distribution governed by an
698 altitudinal gradient and terrain roughness. *Geophysical Research Letters* 38, 2011.

699 Liston, G.E.: Interrelationships among Snow Distribution, Snowmelt, and Snow Cover
700 Depletion: Implications for Atmospheric, Hydrologic, and Ecologic Modeling. *J. Appl.*
701 *Meteorol.*, 38, 1474–1487, 1999.

702 López-Moreno, J.I., and Nogués-Bravo, D.: A generalized additive model for the spatial
703 distribution of snowpack in the Spanish Pyrenees. *Hydrol. Process.*, 19, 3167–3176, 2005.

704 López-Moreno, J.I., Latron, J., and Lehmann, A.: Effects of sample and grid size on the
705 accuracy and stability of regression-based snow interpolation methods. *Hydrol. Process.*, 24,
706 1914–1928, 2010.

707 López-Moreno, J.I., Vicente-Serrano, S.M., Morán-Tejeda, E., Lorenzo-Lacruz, J., Kenawy,
708 A., and Beniston, M.: Effects of the North Atlantic Oscillation (NAO) on combined
709 temperature and precipitation winter modes in the Mediterranean mountains: Observed
710 relationships and projections for the 21st century. *Global Planet. Change*, 77, 62–76, 2011.

711 López-Moreno, J.I., Fassnacht, S.R., Heath, J.T., Musselman, K.N., Revuelto, J., Latron, J.,
712 Morán-Tejeda, E., and Jonas, T.: Small scale spatial variability of snow density and depth
713 over complex alpine terrain: Implications for estimating snow water equivalent. *Adv. Water*
714 *Resour.*, 55, 40–52, 2012a.

715 López-Moreno, J.I., Pomeroy, J.W., Revuelto, J., and Vicente-Serrano, S.M.: Response of
716 snow processes to climate change: spatial variability in a small basin in the Spanish Pyrenees.
717 *Hydrol. Process.*, 27, 2637–2650, 2012b.

718 McCreight, J.L., Slater, A.G., Marshall, H.P., and Rajagopalan, B.: Inference and uncertainty
719 of snow depth spatial distribution at the kilometre scale in the Colorado Rocky Mountains:
720 The effects of sample size, random sampling, predictor quality, and validation procedures.
721 *Hydrol. Process.*, 28, 933–957. 2014.

722 Molotch, N.P., and Bales, R.C.: Scaling snow observations from the point to the grid element:
723 Implications for observation network design. *Water Resour. Res.*, 41, W11421, 2005.

724 Molotch, N.P., Colee, M.T., Bales, R.C., and Dozier, J.: Estimating the spatial distribution of
725 snow water equivalent in an alpine basin using binary regression tree models: the impact of
726 digital elevation data and independent variable selection. *Hydrol. Process.*, 19, 1459–1479,
727 2005.

728 Mott, R., Schirmer, M., Bavay, M., Grünewald, T., and Lehning, M.: Understanding snow-
729 transport processes shaping the mountain snow-cover. *The Cryosphere*, 4, 545–559, 2010.

730 Mott, R., Schirmer, M., and Lehning, M.: Scaling properties of wind and snow depth
731 distribution in an Alpine catchment. *J. Geophys. Res.-Atmos.*, 116, D06106, 2011.

732 Mott, R., Gromke, C., Grünewald, T., and Lehning, M.: Relative importance of advective heat
733 transport and boundary layer decoupling in the melt dynamics of a patchy snow cover.
734 *Advances in Water Resources* 55, 88–97, 2013.

735 Pomeroy, J.W., and Gray, D.M.: Snowcover accumulation, relocation, and management.
736 National Hydrology Research Institute, Saskatoon, Sask., Canada, 1995.

737 Pomeroy, J., Essery, R., and Toth, B.: Implications of spatial distributions of snow mass and
738 melt rate for snow-cover depletion: observations in a subarctic mountain catchment. *Ann.*
739 *Glaciol.*, 38, 195–201, 2004.

740 Prokop, A.: Assessing the applicability of terrestrial laser scanning for spatial snow depth
741 measurements. *Cold Reg. Sci. Technol.*, 54, 155–163, 2008.

742 Prokop, A., Schirmer, M., Rub, M., Lehning, M., and Stocker, M., A comparison of
743 measurement methods: terrestrial laser scanning, tachymetry and snow probing for the
744 determination of the spatial snow-depth distribution on slopes. *Ann. Glaciol.*, 49, 210–216,
745 2008.

746 Revuelto, J., López-Moreno, J.I., Azorin-Molina, C., Zabalza, J., Arguedas, G., and Vicente-
747 Serrano, S.M.: Mapping the annual evolution of snow depth in a small catchment in the
748 Pyrenees using the long-range terrestrial laser scanning. *Journal of Maps*, 1–15., DOI:
749 10.1080/17445647.2013.869268, 2014.

750 Schaffhauser, A., Adams, M., Fromm, R., Jörg, P., Luzi, G., Noferini, L., and Sailer, R.:
751 Remote sensing based retrieval of snow cover properties. *Cold Reg. Sci. Technol.*, 54, 164–
752 175, 2008.

753 Schirmer, M., and Lehning, M.: Persistence in intra-annual snow depth distribution: 2. Fractal
754 analysis of snow depth development. *Water Resour. Res.*, 47, W09517, 2011.

755 Schirmer, M., Wirz, V., Clifton, A., and Lehning, M.: Persistence in intra-annual snow depth
756 distribution: 1. Measurements and topographic control. *Water Resour. Res.*, 47, W09516,
757 2011.

758 Scipión, D.E., Mott, R., Lehning, M., Schneebeli, M., and Berne, A.: Seasonal small-scale
759 spatial variability in alpine snowfall and snow accumulation. *Water Resour. Res.*, 49, 1446–
760 1457, 2013.

761 Steger, C., Kotlarski, S., Jonas, T., and Schär, C.: Alpine snow cover in a changing climate: a
762 regional climate model perspective. *Clim. Dynam.*, 1–20, 2012.

763 Sturm, M., and Wagner, A.M.: Using repeated patterns in snow distribution modeling: An
764 Arctic example. *Water Resources Research* 46, 2010.

765 Trujillo, E., Ramírez, J.A., and Elder, K.J.: Topographic, meteorologic, and canopy controls
766 on the scaling characteristics of the spatial distribution of snow depth fields. *Water Resour.*
767 *Res.*, 43, W07409, 2007.

768 Watson, F.G.R., Anderson, T.N., Newman, W.B., Alexander, S.E., and Garrott, R.A.:
769 Optimal sampling schemes for estimating mean snow water equivalents in stratified
770 heterogeneous landscapes. *Journal of Hydrology* 328, 432–452, 2006.

771 Weiss, A.D.: Topographic position and landforms analysis. ESRI user conference, San Diego
772 USA, 2001.

773 Willmott, C.J. On the Validation of Models. *Phys. Geogr.*, 2, 184–194, 1981.

774 Winstral, A., and Marks, D.: Simulating wind fields and snow redistribution using terrain-
775 based parameters to model snow accumulation and melt over a semi-arid mountain
776 catchment. *Hydrol. Process.*, 16, 3585–3603, 2002.

777 Winstral, A., Elder, K., and Davis, R.E.: Spatial Snow Modeling of Wind-Redistributed Snow
778 Using Terrain-Based Parameters. *Journal of Hydrometeorol.*, 3, 524–538, 2002.

779 Winstral, A., and Marks, D.: Long-term snow distribution observations in a mountain
780 catchment: Assessing variability, time stability, and the representativeness of an index site.
781 *Water Resour. Res.* 50, 293–305, 2014.

782 Wipf, S., Stoeckli, V., and Bebi, P.: Winter climate change in alpine tundra: plant responses
783 to changes in snow depth and snowmelt timing. *Climatic Change*, 94, 105–121, 2009.

784
785
786
787
788
789
790

791 **9. Tables**

	Snow season 2012						Snow season 2013					
	22/02	02/04	17/04	02/05	14/05	24/05	17/02	03/04	25/04	06/06	12/06	20/06
Mean SD (m)	0.72	0.58	0.60	0.97	0.71	0.70	2.98	3.22	2.53	2.28	2.09	1.61
Max SD (m)	5.5	3.8	5.3	6.1	4.4	4.3	10.9	11.2	10.1	9.6	8.9	7.9
SCA (%)	67.2	33.5	94.1	98.8	30.9	18.9	98.8	100.0	96.3	86.4	77.1	67.0

792

793 **Table 1:** Summary statistics of the snowpack distribution and the snow covered area of the
 794 basin. Note that snow covered area is expressed as a % of the total area surveyed by the TLS,
 795 and the mean SD is the average of all SDs not including zero values.

	Snow season 2012						Snow season 2013					
	22/02	02/04	17/04	02/05	14/05	24/05	17/02	03/04	25/04	06/06	12/06	20/06
Sx 0°	0.19	0.13	0.09	-0.11	0.06	-0.01	0.51*	0.40*	0.31*	0.23*	0.22*	0.20*
Sx 45°	0.15	-0.02	0.00	-0.16	-0.08	-0.09	0.36*	0.25*	0.17	0.12	0.12	0.12
Sx 90°	0.12	-0.14	-0.07	0.11	-0.11	-0.03	-0.15	-0.15	-0.10	-0.09	-0.09	-0.10
Sx 135°	0.02	-0.05	0.05	0.26*	0.01	0.11	-0.27*	-0.19	-0.10	-0.06	-0.06	-0.06
Sx 180°	0.02	0.14	0.15	0.38*	0.17	0.21*	-0.19	-0.08	0.02	0.08	0.08	0.12
Sx 225°	0.12	0.29*	0.26*	0.44*	0.32*	0.23*	0.06	0.18	0.26*	0.29*	0.29*	0.31*
Sx 270°	0.20*	0.33*	0.34*	0.26*	0.27*	0.21*	0.48*	0.52*	0.49*	0.45*	0.42*	0.43*
Sx 315°	0.22*	0.26*	0.27*	0.01	0.22*	0.12	0.56*	0.50*	0.41*	0.34*	0.32*	0.33*

796

797 **Table 2:** Pearson’s r coefficients between SD and Sx, calculated for the eight studied wind
 798 directions over the survey days. * marks those correlations that were statistically significant
 799 ($\alpha < 0.05$) in at least the half of the samples (500 out of 1000 samples) from the Monte Carlo
 800 approach, and bold r coefficients represent the best correlated Sx direction for a specific
 801 survey day.

802

803

804

	Snow season 2012						Snow season 2013					
	22/02	02/04	17/04	02/05	14/05	24/05	17/02	03/04	25/04	06/06	12/06	20/06
Elev.	0.09	0.26*	0.16	0.10	0.29*	0.19	0.09	0.18	0.13	0.18	0.21*	0.26*
Slope	0.06	0.18	0.02	-0.03	0.20*	0.03	0.25*	0.27*	0.20*	0.20*	0.21*	0.26*
Curv	-0.44*	-0.45*	-0.47*	-0.49*	-0.41*	-0.37*	-0.39*	-0.40*	-0.40*	-0.39*	-0.38*	-0.38*
North	-0.06	0.00	0.04	0.19	0.07	0.11	-0.38*	-0.27*	-0.19	-0.09	-0.06	-0.11
East.	0.09	0.21*	0.13	0.13	0.13	0.11	0.25*	0.26*	0.27*	0.22*	0.18	0.14
Rad	0.05	0.04	-0.06	-0.22*	-0.12	-0.11	0.36*	0.21*	0.10	-0.09	-0.12	-0.23*
TPI 25	-0.56*	-0.46*	-0.54*	-0.58*	-0.40*	-0.32*	-0.66*	-0.68*	-0.68*	-0.66*	-0.63*	-0.61*
Sx	0.22*	0.33*	0.34*	0.44*	0.32*	0.23*	0.56*	0.52*	0.49*	0.45*	0.42*	0.43*

805

806 **Table 3:** Pearson's r coefficients between SD and the topographic variables. * marks those
807 correlations that were statistically significant ($\alpha < 0.05$) in at least the half of the samples (500
808 out of 1000 samples) from the Monte Carlo approach, and bold r coefficients represent the
809 best correlated topographic variable for a specific survey day.

810

	Snow season 2012						Snow season 2013					
	22/02	02/04	17/04	02/05	14/05	24/05	17/02	03/04	25/04	06/06	12/06	20/06
TPI	-0.69	-0.53	-0.60	-0.59	-0.48	-0.40	-0.78	-0.72	-0.73	-0.80	-0.74	-0.72
Sx		0.11	0.28	0.26	0.20	0.16	0.36	0.31	0.43	0.37	0.38	0.31
Elev.	0.09	0.22	0.34	0.27	0.27	0.35		0.14		0.08		0.13
Slope		-0.25	-0.29	-0.24	-0.21	-0.21		-0.10	-0.14	-0.16	-0.09	-0.15
North	-0.22	0.13	-0.16				-0.12	-0.11	-0.11			
East.	0.10						0.29	0.25	0.25	0.31	0.23	0.20
r2	0.45	0.31	0.40	0.47	0.33	0.25	0.65	0.63	0.60	0.60	0.57	0.51

811

812 **Table 4:** Multiple linear regression beta coefficients for each independent variable and
813 sampled day.

814

815

816

817

818

819

	Snow season 2012						Snow season 2013					
	22/02	02/04	17/04	02/05	14/05	24/05	17/02	03/04	25/04	06/06	12/06	20/06
TPI	83.2	78.8	75.0	71.7	74.0	66.9	49.1	56.4	64.4	71.2	69.9	77.5
Sx			4.6	12.7	13.4	10.8	45.9	23.1	23.0	21.8	20.1	12.5
Elev.	5.7	6.8	13.2	9.1	8.2	15.2	5.0	5.7	5.0	3.3	5.9	5.4
Slope	1.7	5.4	5.7	6.5	3.2	7.0			2.1			
North	9.3	8.1	1.5		1.3			14.7	4.3	2.4	2.9	3.6
East.									1.2	1.3	1.1	1.0
r2	0.56	0.42	0.52	0.54	0.46	0.39	0.58	0.56	0.55	0.54	0.53	0.51

820

821 **Table 5:** Contribution of the various topographic variables to the explained variance of SD

822 distribution in the binary regression tree models for 2012 and 2013. Values have been

823 rescaled from 0 to 100.

824

825

826

827

828

829

830

831

832

833

834

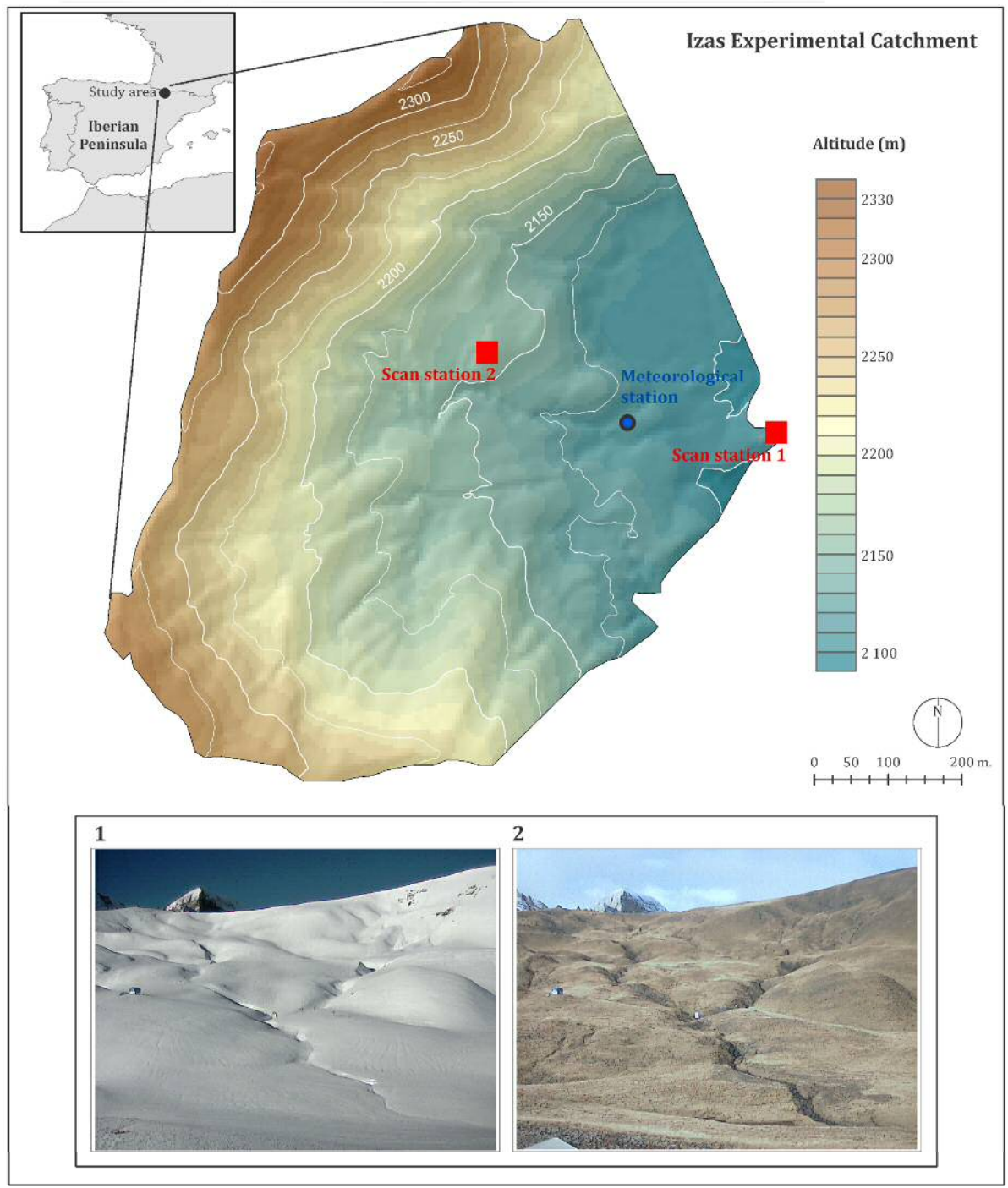
835

836

837

838

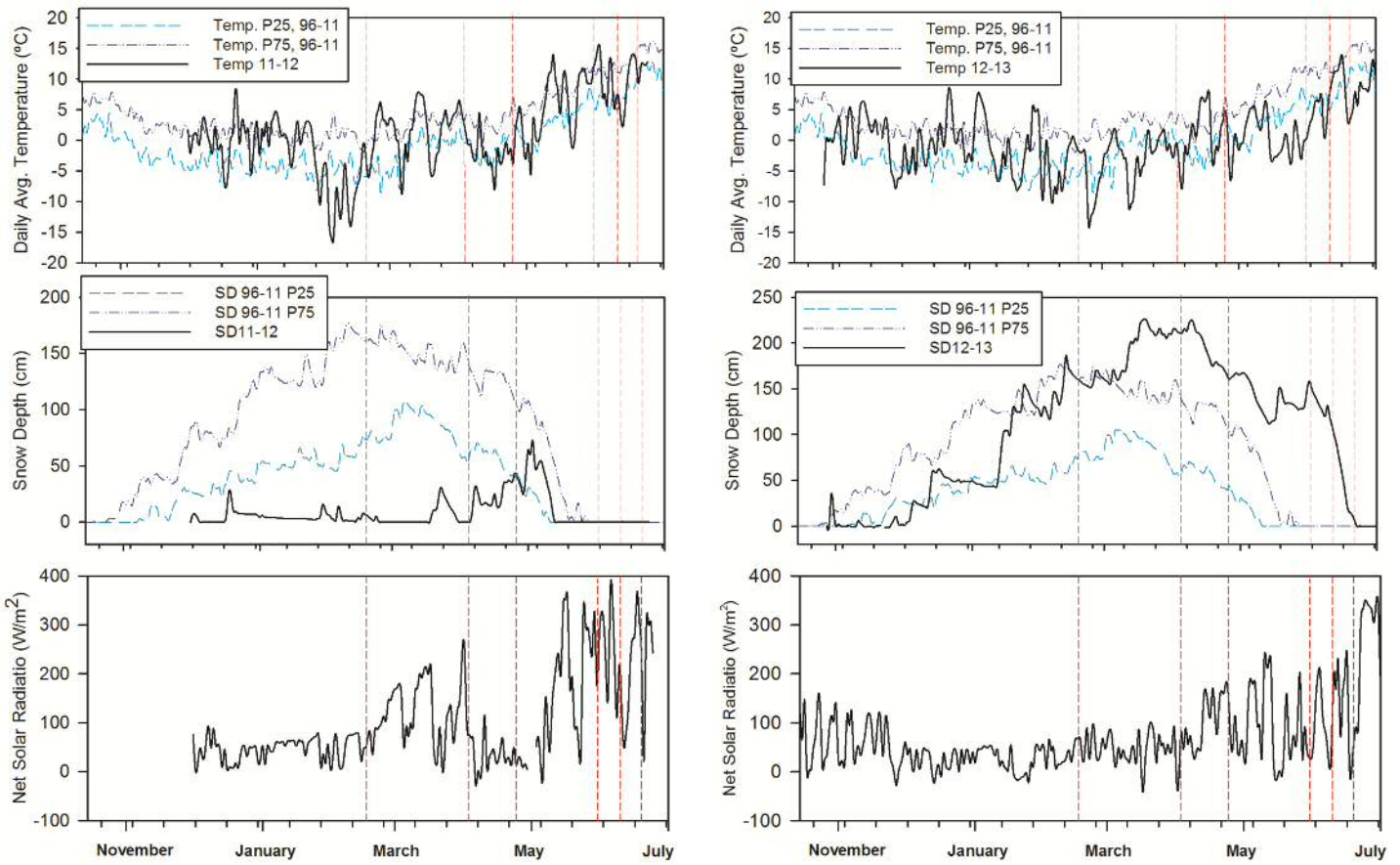
839



841

842 **Figure 1:** Location of the Izas experimental catchment, and the digital elevation model
843 showing the positions of the scan stations and the automatic meteorological station. The two
844 images in the bottom part of the figure, from Scan Station 1, show the terrain characteristics
845 with (1) and without snow cover (2).

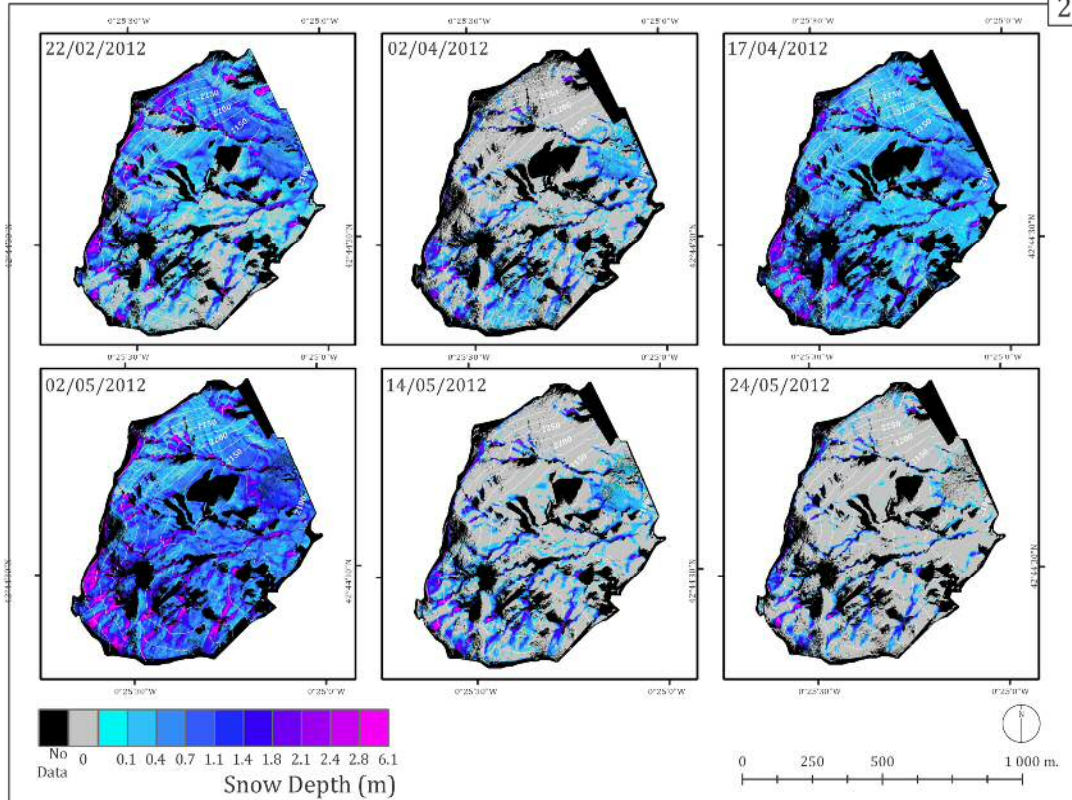
846



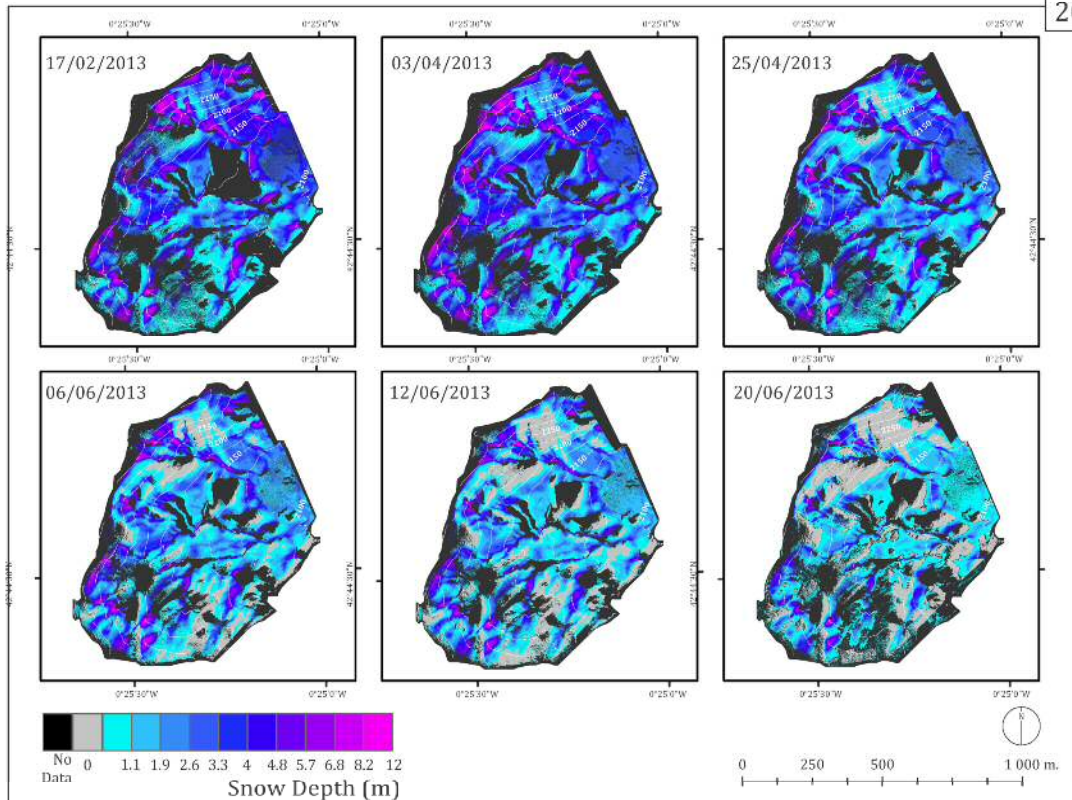
849 **Figure 2:** Daily average temperature, snow depth and net solar radiation (short wave) at the
 850 automatic weather station (AWS) for the 2012 (left) and 2013 (right) snow seasons. The
 851 continuous lines represent the daily values for 2012 and 2013, and the dashed lines show the
 852 25th and 75th percentiles of historical daily series (1996–2011). The vertical dashed lines
 853 show the TLS survey days. Note that during some surveys no snow was present at the AWS,
 854 but some areas of the Izas experimental catchment were covered by snow.

Snow Depth in Izas Experimental Catchment

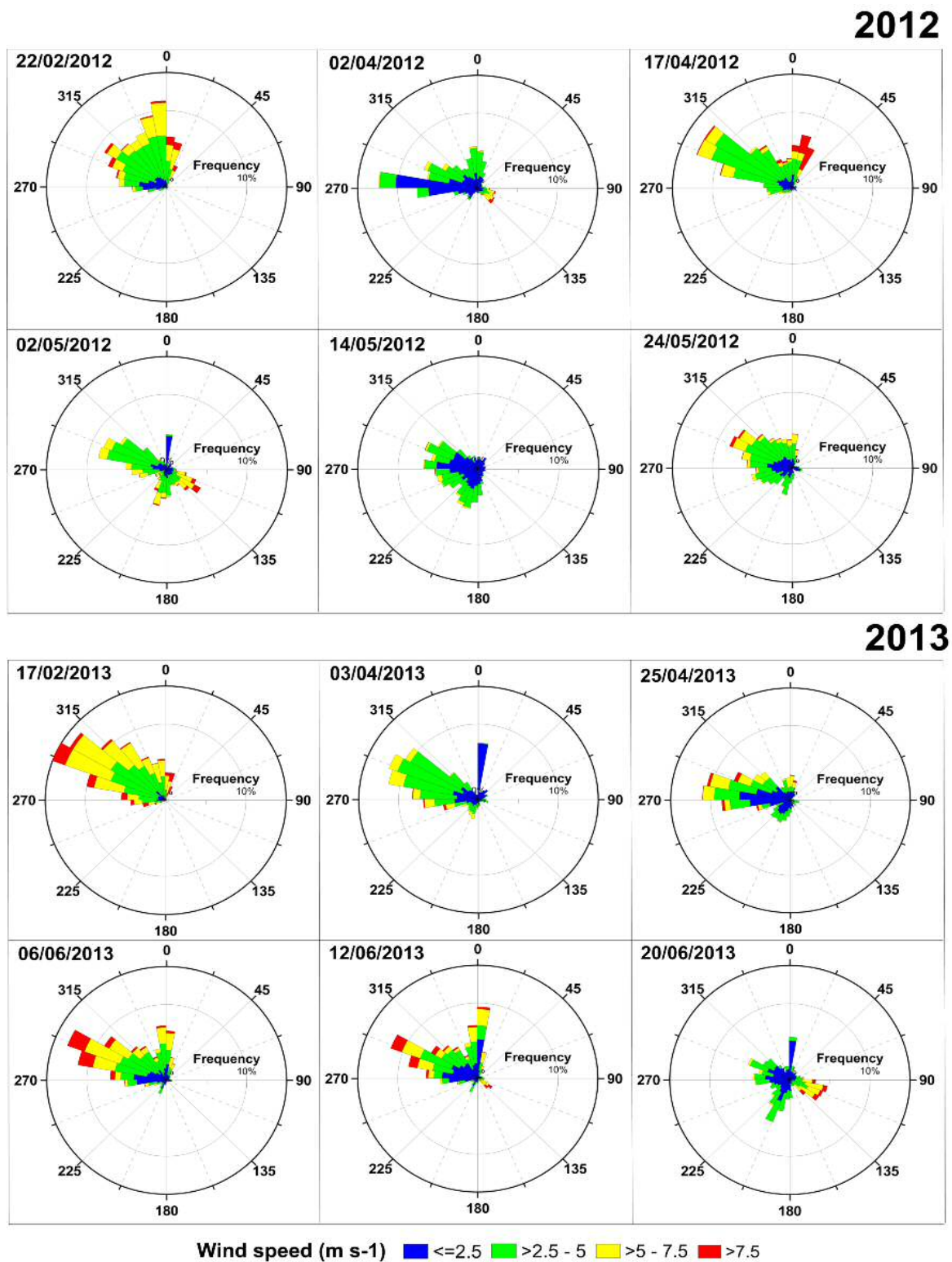
2012



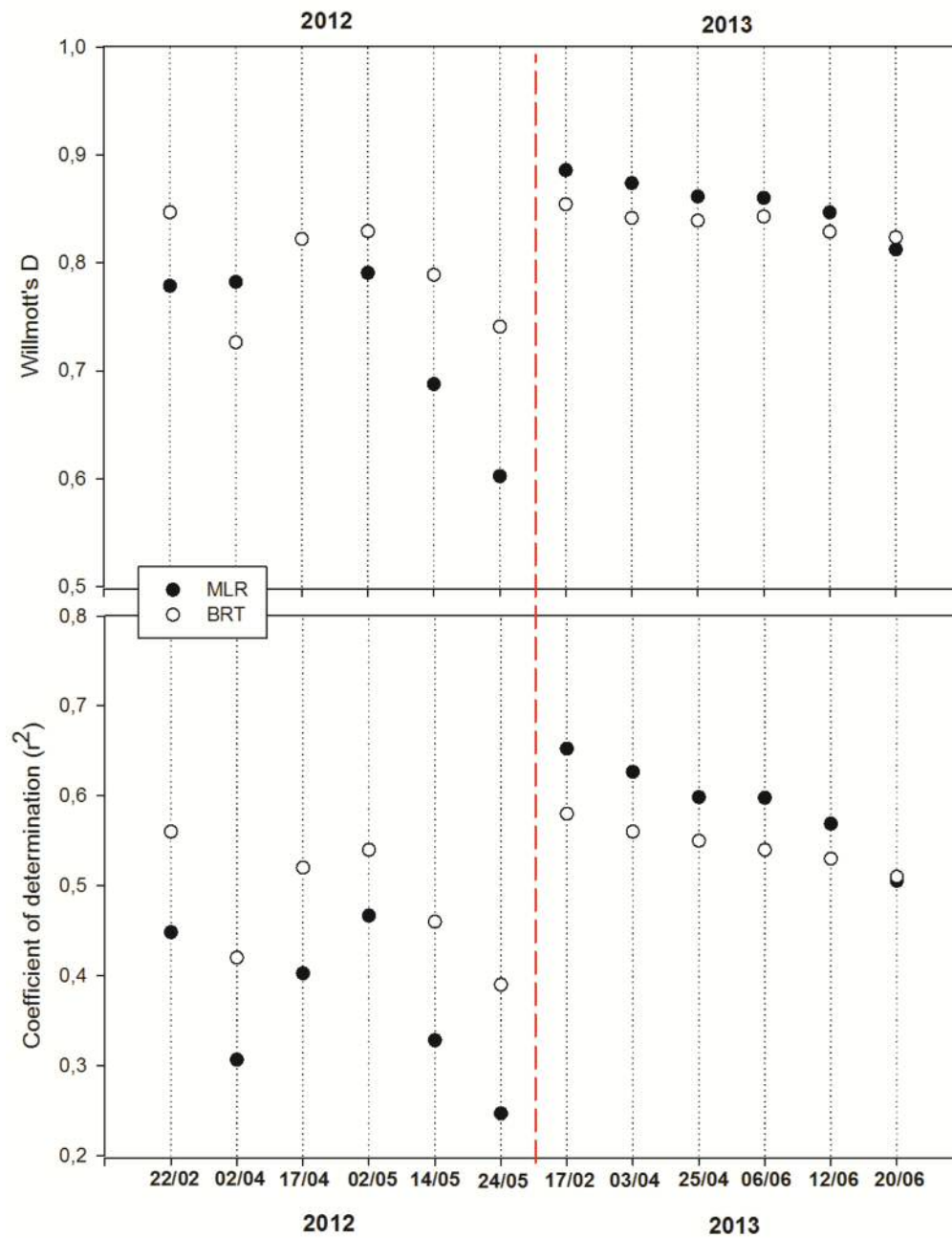
2013



860 **Figure 3:** Spatial distribution of snow depth in the Izas experimental catchment in the surveys
 861 undertaken in 2012 and 2013.



862
 863 **Figure 4:** Wind roses from the automatic weather station placed at the catchment obtained for
 864 a 15 day period.

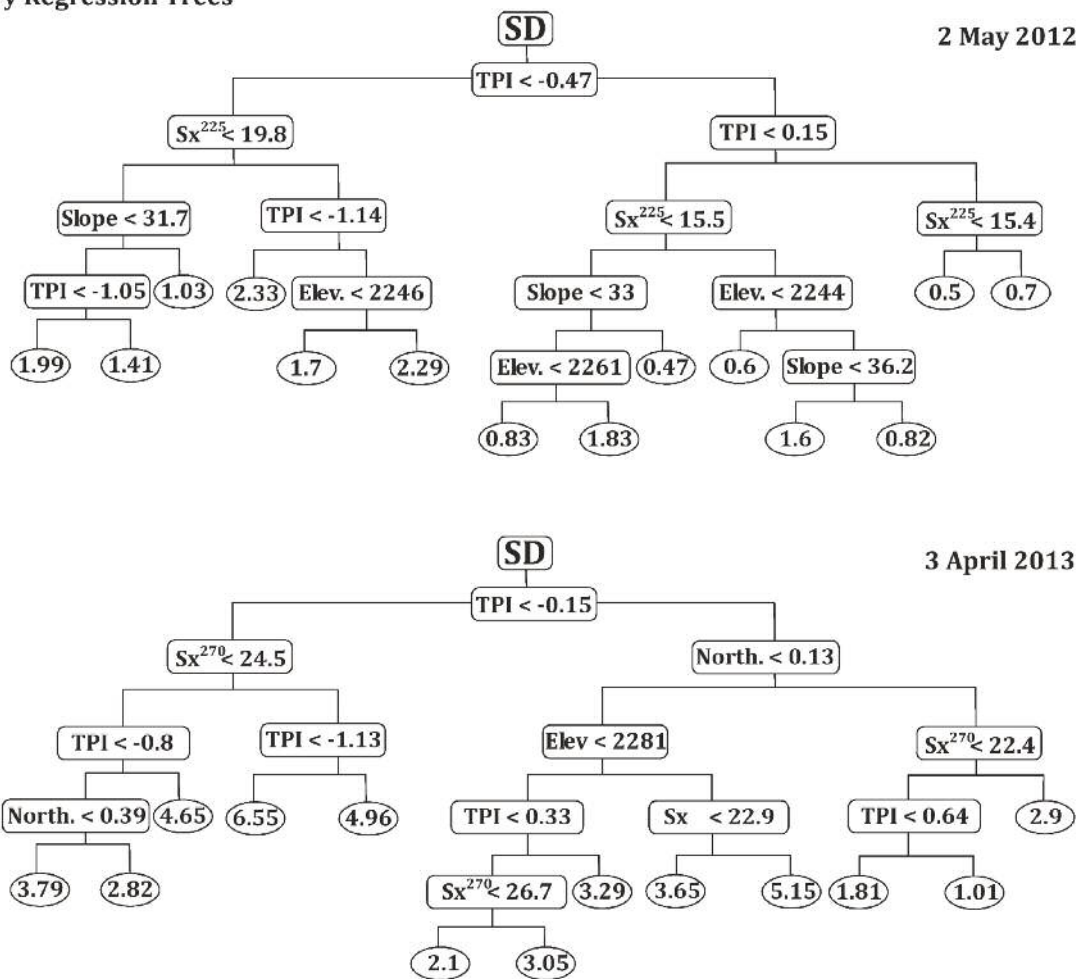


865

866 **Figure 5:** Willmott's D and r^2 values between the observed and predicted SD, based on the
 867 multiple linear and binary regression models for all survey days.

868

Binary Regression Trees



869

870 **Figure 6:** Binary regression tree obtained for 2 May 2012(top) and 3 April 2013 (bottom).

871 The final nodes (with ellipses) show the predicted SD in the zone having the specified terrain

872 characteristics. At each branch point, one topographic variable is considered; if the value is

873 less than the specified value, the left branch is selected, but if it is equal to or greater than the

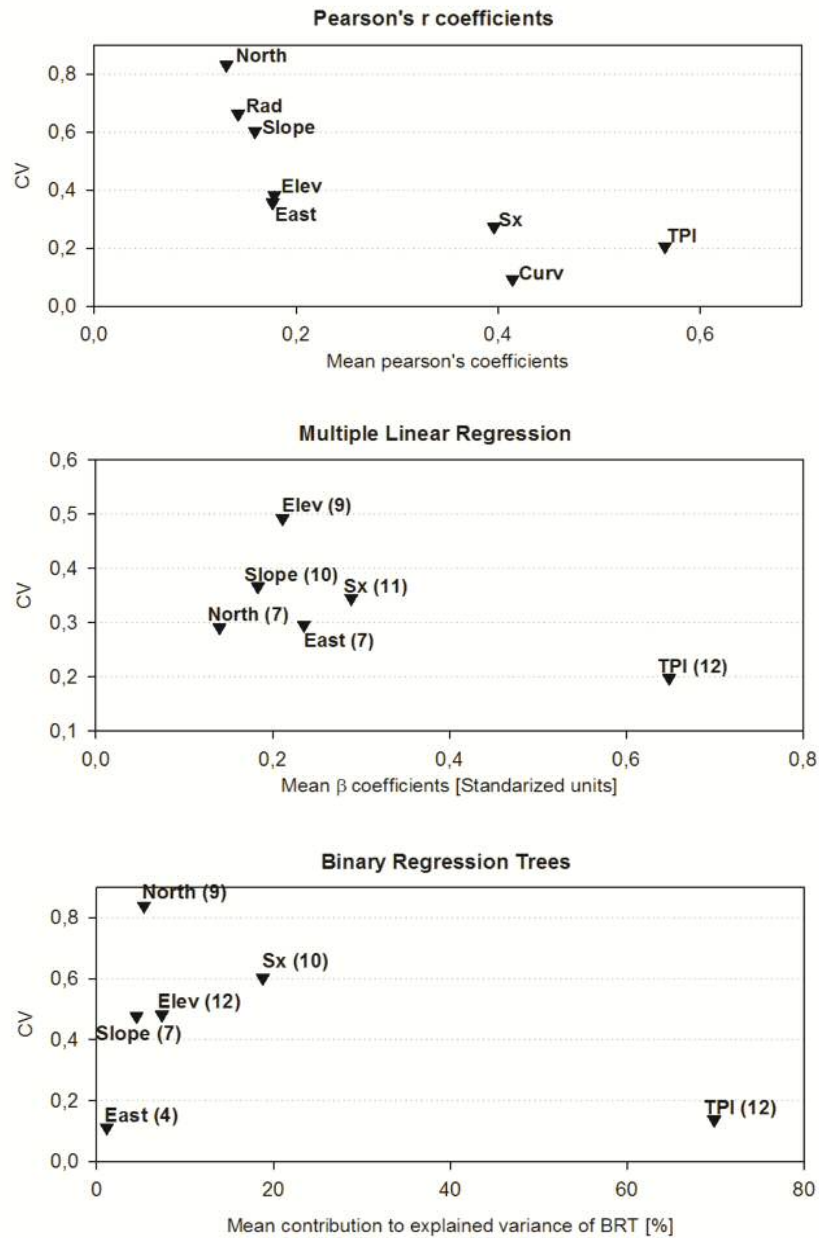
874 specified value, the right branch is selected.

875

876

877

878



879

880 **Figure 7:** Mean contribution of topographic variables to models and Pearson's r coefficients
 881 versus the coefficients of variation for all considered surveys. Upper panel shows Pearson's r
 882 coefficients; middle panel shows beta coefficients of the Multiple Linear Regression; and the
 883 bottom panel shows the contribution to the explained variance to the Binary Regression Trees.
 884 Each graph point is accompanied with its variable, and in the case of MLR and BRT, in
 885 brackets the number of days in which each variable was included in models.